https://doi.org/10.5194/egusphere-2026-5590
Preprint. Discussion started: 10 November 2026
© Author(s) 2026. CC BY 4.0 License.

Measurement report: In situ analysis of aerosol properties and its effects on cloud-fog in Liupan Mountains

Run Luo[1, 2], Zhiliang Shu[1, 2 *], Zhuolin Chang[1, 2], Fusheng Li[1, 2], Le Jia[1, 2], Jianhua Mu[1, 2], Lei Tian[1, 2], Zhangli Dang[1, 2], Longyan Li[1, 2], Liren Xu[3], Zezhong Sun[3], Yuzhi Liu[4 *]

[1]Guyuan Field Research Station for Weather Modifcation and Cloud Physics, China Meteorological Administration, Yinchuan 750002, China
[2]Liupanshan Atmospheric Science Field Observation and Research Station in Ningxia Hui Autonomous Region, Yinchuan 750002, China
[3]State Key Laboratory of Spatial Datum, Xi'an 710054, China
[4]Key Laboratory for Semi-Arid Climate Change of the Ministry of Education, Lanzhou University, Lanzhou 730000, China

Correspondence to: Zhiliang Shu (8633204@163.com) and Yuzhi Liu (liuyzh@lzu.edu.cn)

Abstract. Aerosols play a crucial role in cloud and fog formation as cloud condensation nuclei (CCN), yet their characteristics and activation behavior over the complex terrain of the Liupan Mountain (LM) area remain poorly understood. Based on long-term in situ observations in the LM area, this study systematically analyzed submicron aerosol size distribution, activation behavior, and their impacts on cloud and fog microphysics. The results show that submicron aerosol number concentration (N_a) peaks in late autumn and late spring and exhibits an afternoon unimodal distribution, whereas mass concentration (M_a) reaches its maximum in early August, mainly contributed by accumulation mode particles. The aerosol size distribution exhibits marked weather-dependent shifts, transitioning from bimodal new-particle formation on clear days to accumulation-mode growth under foggy conditions and Aitken-mode dominance after wet scavenging on rainy days. Importantly, N_a varies synchronously with CCN number concentration (N_{CCN}), and accumulation mode particles serve as the dominant CCN source. Consequently, N_a is positively correlated with fog droplet number concentration (N_f) but negatively correlated with droplet size and liquid water content (LWC), leading to a "many but small" fog droplet spectrum under high aerosol loading. Observations of a typical fog event reveal a two-way feedback. Aerosols supply CCN for fog formation, while the activation, growth, and evaporation of fog droplets in turn modify aerosol concentration and size distribution. These findings provide critical in situ evidence for understanding mountain fog formation and the indirect effects of aerosols.

Keywords. Aerosol; Size Distribution; Cloud-Fog Microphysics; Liupan Mountains

1 Introduction

Atmospheric aerosols are a general term for solid and liquid particles suspended in the atmosphere. Based on their emission sources, they can be classified into natural and anthropogenic sources, and are widely involved in various atmospheric physical processes such as cloud-precipitation, radiative transfer, and atmospheric photoelectric phenomena (Bellouin et al.,

https://doi.org/10.5194/egusphere-2026-5590
Preprint. Discussion started: 10 November 2026
© Author(s) 2026. CC BY 4.0 License.

2020; Zhang et al., 2024). On the one hand, aerosols can exert direct effects by absorbing and scattering solar shortwave radiation, as well as emitting and trapping longwave radiation (Li et al., 2022; Zhang et al., 2022a). On the other hand, aerosols can effectively serve as cloud condensation nuclei (CCN) and ice nuclei (IN), modifying cloud microphysical properties and thereby altering cloud albedo and lifetime, producing an indirect effects (Liu et al., 2020; Luo et al., 2023). Aerosol indirect effects include the Twomey effect (first indirect effect) and the Albrecht effect (second indirect effect). The former manifests as an increase in aerosol concentration that enhances cloud droplet number concentration while reducing droplet effective radius, thereby elevating cloud albedo under fixed liquid water path (Twomey, 1974; Twomey, 1977; Quaas et al., 2020; Zhang et al., 2022b). The latter is characterized by the suppression of raindrop formation and the delay of precipitation onset due to reduced droplet size, which consequently alters cloud lifetime (Albrecht, 1989; Jung et al., 2020; Li et al., 2025). Through these direct and indirect effects, aerosols continuously modulate the radiative budget of the Earth system (Rosenfeld et al., 2008; Barahona et al., 2011; Dagan et al., 2023), influence cloud and precipitation processes (Fan et al., 2018; Hua et al., 2020; Adhikari and Mejia, 2023), and ultimately affect the hydrological cycle as well as regional and global climate (Storelvmo and Tan, 2015; Huang et al., 2017). These multifaceted aerosol effects thus constitute a central and unresolved frontier in contemporary weather and climate research. The Sixth Assessment Report (AR6) of the Intergovernmental Panel on Climate Change (IPCC) pointed out that aerosol-cloud interactions represent the largest uncertainty in the current assessment of anthropogenic radiative forcing (IPCC, 2021). Therefore, conducting systematic investigations of aerosol properties and their impacts on cloud microphysical processes in representative regions is of crucial importance for improving regional climate prediction capabilities and optimizing weather modification strategies.

The Liupan Mountain (LM) is located in the transitional zone between the northeastern margin of the Tibetan Plateau and the Loess Plateau. It serves as a core water conservation area for nearly ten million people in Ningxia and its surrounding regions, and also constitutes a critical ecological barrier for the Yellow River Basin, possessing a strategic position of paramount ecological and hydrological significance (Lin et al., 2022; He et al., 2023). The mountain range is oriented nearly north-south, extending approximately 200 km in length and 50 km in width, with its highest peak, Mt. Miguanshan, reaching an altitude of 2942 m. The pronounced topographic relief give rise to intense dynamic uplift (Cao et al., 2023). Owing to its unique geographical location, this region is simultaneously governed by the East Asian monsoon, the westerly circulation, and the plateau monsoon. The interplay of these three major weather systems gives rise to complex local thermodynamic and dynamic processes, resulting in abundant orographic cloud and fog resources (Lin et al., 2025; Chang et al., 2026). Compared with plateaus and plains, the LM features a moderate orographic scale, typical cloud/fog processes, and unique local meteorological conditions. Influenced by both natural emissions and anthropogenic aerosol transport, the aerosol physicochemical properties in this region are complex, and their coupling with orographic clouds and fog is pronounced. Therefore, systematically investigating aerosol properties and their influence mechanisms on the evolution and microphysical characteristics of clouds and fog in this region is of great value for advancing our scientific understanding of aerosol indirect effects under complex terrain conditions.

https://doi.org/10.5194/egusphere-2026-5590
Preprint. Discussion started: 10 November 2026
© Author(s) 2026. CC BY 4.0 License.

In recent years, numerous studies have been conducted on the effects of aerosols on clouds and fog, confirming that aerosol concentration, size distribution, and chemical composition are key factors regulating cloud and fog microphysical and optical properties, and that they can significantly alter cloud droplet activation efficiency as well as the generation, development, and dissipation of clouds and fog (Liu et al., 2023; Motos et al., 2023; Li et al., 2025). Currently, aerosol-cloud/fog related studies are primarily carried out using a variety of techniques, including ground-based in situ observations (Duan et al., 2023; Gao et al., 2025; Zhang et al., 2026), aircraft measurements (Wehbe et al., 2021; Fast et al., 2024), and numerical modeling (Singh et al., 2024; Barman and Gokhale, 2022), which have laid a solid theoretical and observational foundation for understanding the cloud-related effects of atmospheric aerosols over different underlying surfaces. In terms of field observational campaigns, extensive systematic studies have been conducted across various mountainous regions. For example, the RACLETS (Role of Aerosols and Clouds Enhanced by Topography on Snow) field experiment was carried out in the Swiss Alps during February to March 2019, utilizing combined aircraft and ground-based measurements to obtain high-resolution data on cloud and aerosol properties, and systematically analyzed the impact of aerosol CCN activity on cloud droplet formation (Georgakaki et al., 2021). In the Colorado Rocky Mountains of the United States, the SAIL (Surface-Atmosphere Integrated field Laboratory) large-scale comprehensive field campaign was implemented in the East River watershed from 2021 to 2023, conducting systematic observations of boundary layer structure, cloud-boundary layer stratification relationships, and aerosol impacts on snowmelt processes under complex terrain conditions (Feldman et al., 2023). The SAIL-Net distributed measurement network further revealed the spatiotemporal variability of aerosol, CCN, and INP concentrations in mountainous terrain (Gibson et al., 2025). In China, mountain observations have also accumulated substantial findings. Xu et al. (2024) carried out synchronous observations of aerosol and CCN at two sites on the northeastern edge of the Tibetan Plateau, revealing that both sites dominated by sulfate and organic aerosols and exhibiting high hygroscopicity parameters, confirming the significant impact of anthropogenic aerosol transport on CCN concentration and activity in the Qilian Mountain region. Ji et al. (2025) conducted in situ observations of aerosol activation properties during the South Asian summer monsoon, revealing that aerosol activation was significantly suppressed by monsoon-induced modulation of aerosol and moisture transport.

In terms of numerical modeling, the WRF-Chem model has become a critical tool for investigating aerosol impacts on orographic clouds and precipitation. Henao et al. (2023) applied a cloud-resolving WRF-Chem configuration at 3 km resolution to analyze the impacts of anthropogenic aerosols from the Phoenix urban area on orographic precipitation in the surrounding mountains of Arizona, finding that aerosols decreased frozen precipitation on the windward side by approximately 9% while increasing it on the lee side by about 8%. Yang et al. (2016) employed convection-permitting WRF-Chem simulations to explore the mechanisms governing precipitation changes from orographic clouds in the Mt. Hua area of central China, revealing that anthropogenic pollution contributed to a roughly 40% reduction in precipitation over Mt. Hua during a one-month summertime period, primarily through absorbing aerosol-induced radiative heating that weakened the valley breeze circulation and reduced water vapor transport from the valley to the mountain. Adhikari and Mejia (2022)

https://doi.org/10.5194/egusphere-2026-5590
Preprint. Discussion started: 10 November 2026
© Author(s) 2026. CC BY 4.0 License.

implemented a convection-permitting WRF-Chem configuration to assess the impact of long-range transported dust aerosols on precipitation and convective processes over the Nepal Himalayas, finding that dust aerosols enhanced precipitation by 9.6% over mountainous terrains through activation as cloud condensation nuclei that increased droplet concentration and enhanced convection via latent heat release. Despite the significant progress made through both observational and modeling studies in recent years, the vast majority of research efforts concerning aerosol properties in mountainous regions have been overwhelmingly concentrated on the Tibetan Plateau, the Himalayas, and the Rocky Mountains. In stark contrast, the LM area, which is situated precisely in the transitional zone between the Loess Plateau and the Tibetan Plateau, remains virtually uncharted with respect to its aerosol physicochemical characteristics and their regulatory effects on the microphysical evolution of orographic clouds and fog.

In this study, we investigated the multi-timescale evolution of submicron aerosols, their size distribution characteristics under different weather conditions, as well as their activation properties and subsequent effects on cloud and fog microphysical processes, using multi-source in situ observations. Descriptions of the datasets are provided in Sections 2. In Section 3, the characteristics of submicron aerosol variations over different time scales in the Liupan Mountain are described. In Section 4, the characteristics of submicron aerosol size distribution under different weather conditions are analyzed. In Section 5, the impact of submicron aerosols on clouds and fog is presented. The main conclusion and discussion are presented in Section 6.

2 Datasets

In this study, multiple high-precision in-situ instruments were deployed for synchronous observations. The observation site is located at the LM Meteorological Station (106.12°E, 35.40°N). The specific location and the surrounding environment of the observation instruments are shown in Figure 1.

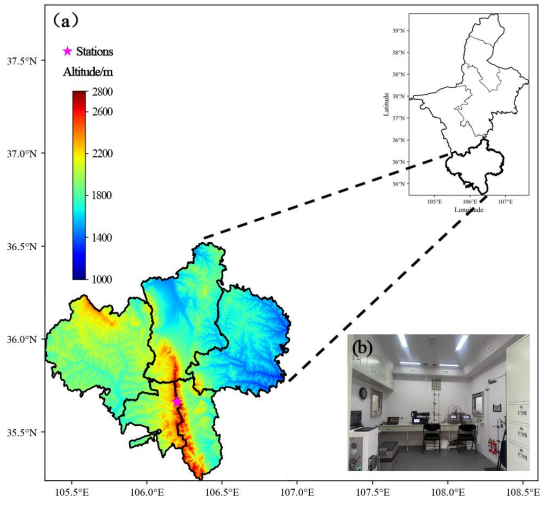


Figure 1: (a) Geographic location of the observation site and the surrounding terrain altitude (unit: m), and (b) schematic diagram of the observation instrument environment.

https://doi.org/10.5194/egusphere-2026-5590
Preprint. Discussion started: 10 November 2026
© Author(s) 2026. CC BY 4.0 License.

A Scanning Mobility Particle Sizer (SMPS) was used to obtain the size distribution and number concentration of submicron aerosols. The instrument has an effective measurement size range of 4-1000 nm, with a full-size scan cycle of approximately 7 minutes. The SMPS mainly consists of two core modules, namely a Differential Electrical Mobility Classifier (DEMC) and a Condensation Particle Counter (CPC). A large-flow drying tube is installed at the instrument inlet to reduce the humidity of the sampled air. The aerosol sample first passes through a neutralizer to achieve charge equilibrium, then enters the DEMC for precise size selection, and is finally counted by the CPC, thereby outputting high-resolution number size distribution data. For this study, continuous SMPS observations from September 2024 to August 2025 were used to systematically analyze the multi-timescale evolution characteristics of submicron aerosols in the study area, including diurnal and seasonal variations.

Cloud condensation nuclei (CCN) observations were conducted using a CCN-100 cloud condensation nuclei counter. The instrument calculates the number concentration of CCN based on a standard sampling flow rate and can measure CCN particles within a size range of 0.75 to 10 μm. The size channels of the instrument adopt a non-uniform width design. Channel Bin1 covers a size interval of 0 to 0.75 μm, Channel Bin2 covers 0.75 to 1.0 μm, and channels for particle sizes larger than 1.0 μm are divided with a uniform step size of 0.5 μm up to 10.0 μm. This design fully covers the typical size range of cloud and fog activated particles in the study area. The instrument has a sampling frequency of 1 second. A total of five supersaturation levels were set, namely 0.2%, 0.4%, 0.6%, 0.8%, and 1.0%, with a complete observation cycle covering all supersaturation levels taking one hour. In this study, continuous CCN observation data from September 1 to 21, 2024, were selected to quantitatively analyze the regional aerosol activation efficiency and the differences in the contributions of different modes under varying supersaturation levels.

A FM-120 fog droplet spectrometer was used to simultaneously observe cloud-fog microphysical parameters and to investigate the feedback mechanism between aerosols and cloud-fog. The instrument covers droplet sizes from 2 to 50 μm, with a sampling area of 0.24 mm^2 and a temporal resolution of 1 second. The spectrometer uses a solid state laser diode as the core detection element, and based on the principle of laser forward scattering, retrieves key microphysical parameters in real time, including droplet size distribution, droplet number concentration, liquid water content, and droplet median volume diameter. In addition, observational data from a DNQ1 scattering visibility meter collected during September 1 to September 30, 2024, together with relative humidity and precipitation records from the Liupan Mountain National Automatic Weather Station, were integrated to select typical fog and precipitation events. These data were then used to analyze the variations in aerosol size distribution under different weather conditions.

3 Characteristics of submicron aerosol variations over different time scales in the Liupan Mountain area

Figure 2 presents the time series of submicron aerosol number concentration (N_a) and aerosol mass concentration (M_a) from September 2024 to August 2025. From the perspective of year-round daily variations, both the N_a and M_a in the LM area exhibit pronounced seasonal fluctuations, with clearly different timings for their respective peaks. High N_a values are concentrated in late autumn and late spring. During October to November and from mid April to May, N_a repeatedly

https://doi.org/10.5194/egusphere-2026-5590
Preprint. Discussion started: 10 November 2026
© Author(s) 2026. CC BY 4.0 License.

stabilizes above 3000 cm^{-3}. High M_a values are distributed over three periods, which are August to September, November to December, and mid April to May, with the annual peak reaching 12.0 μg/m^3 in early August. In late autumn, N_a is high while M_a remains only moderate, reflecting the dominance of small particles during this period. From January to early April, both concentrations simultaneously drop to their annual minimum, with the lowest N_a reaching only 51.6 cm^{-3} and M_a generally below 1 μg/m^3. Entering May, N_a rises rapidly again. Subsequently, during the concentrated occurrence period of heavy local topographic rainfall in June and July, efficient wet scavenging leads to a marked decrease in N_a. In contrast, M_a reaches its annual maximum in early August. Overall, N_a and M_a evolve in a staggered pattern of rising and falling peaks, visually reflecting the differences in dominant aerosol processes across seasons.

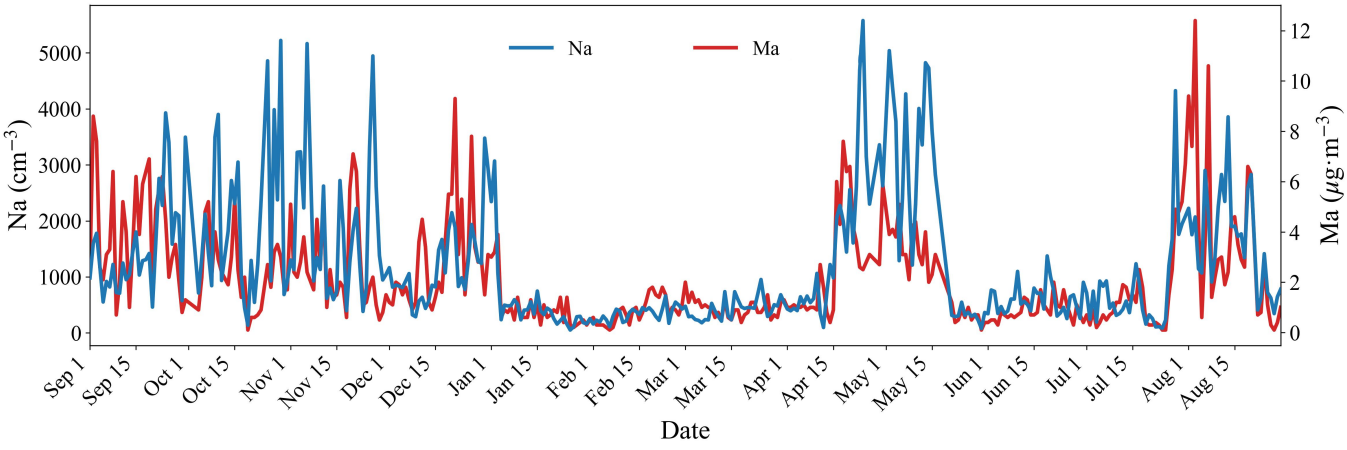


Figure 2: Time series of submicron aerosol number concentration (N_a) and aerosol mass concentration (M_a) from September 2024 to August 2025.

The seasonal differences in aerosol evolution are mainly influenced by particle formation, aging, and removal processes. To further analyze the dominant processes in different seasons, we calculated N_a for different aerosol modes in different seasons (Table 1). In autumn, N_a reaches its annual peak at 1762.88 cm-³, with the nucleation mode fraction also reaching a relatively high value of 23.58%. This indicates that the relatively stable atmospheric diffusion conditions in autumn favor new particle formation (Rowell et al., 2024), leading to a N_a peak dominated by ultrafine particles. However, particle growth during this season is limited, as reflected by the accumulation mode fraction of only 27.92%, and the particle size remains generally small. In winter, dominated by dry and cold air masses, photochemical reactions are significantly suppressed, and N_a drops to the annual minimum of only 688.44 cm^{-3}. During this period, the nucleation mode fraction decreases to 21.42%, whereas the accumulation mode fraction reaches its annual maximum of 31.87%. This suggests that wintertime aerosols are mainly composed of aged and accumulated large particles. Consequently, M_a decreases much less than Na, reflecting the stable contribution of residual particles to the M_a load.

https://doi.org/10.5194/egusphere-2026-5590
Preprint. Discussion started: 10 November 2026
© Author(s) 2026. CC BY 4.0 License.

In spring, as solar radiation intensifies, photochemical reactivity increases, and new particle formation becomes active again (Lehtipalo et al., 2025). N_a rises to 1376.73 cm^{-3}, and the nucleation mode fraction increases correspondingly to 24.84%. In this period, the Aitken mode fraction reaches 54.00%, making it the dominant component of the aerosol. Particles have not yet undergone extensive growth to larger sizes, and the accumulation mode fraction remains at a low annual value of 21.16%. Correspondingly, the seasonal M_a remains at a relatively low level of 1.96 μg/m^3. In summer, N_a decreases to 1020.49 cm^{-3}, and the nucleation mode fraction drops to its annual minimum. This indicates that strong convective activity in summer activates a large number of nucleation mode particles as CCN during cloud formation, and this efficient wet scavenging most effectively removes nucleation mode particles (Ohata et al., 2016; Blanco et al., 2021). Compared with ultrafine particles, the Aitken and accumulation mode particles are less affected by strong wet scavenging. Moreover, given that the site is located in a high humidity environment near cloud base, the remaining particles undergo continuous hygroscopic growth and secondary transformation, leading to a sustained increase in particle size (Deng et al., 2024). As a result, the Aitken mode fraction reaches its annual maximum of 58.33%, and the accumulation mode fraction also remains at a relatively high level of 30.58%. These processes ultimately drive M_a to its annual maximum by the end of summer (Figure 1).

Table 1: Seasonal variations of N_a, M_a, and number fractions of different aerosol modes.

	N_a (cm^{-3})	M_a (ug/m^3)	Nucleation mode (10-20nm, %)	Aitken mode (20-100nm,%)	Accumulation mode (100nm-1um,%)
Autumn	1762.88	2.97	23.58	48.50	27.92
Winter	688.44	1.58	21.42	46.71	31.87
Spring	1376.73	1.96	24.84	54.00	21.16
Summer	1020.49	1.99	11.09	58.33	30.58

Figure 3 presents the diurnal variations of the N_a and M_a, as well as their size distributions. As shown in Figure 3a, the diurnal variation of N_a exhibits typical characteristics of daytime new particle formation. A brief small peak of nucleation mode particles appears around 09:00 local time, followed by a widespread and intensive burst between 12:00 and 18:00, with the peak concentrated in the 10-50 nm size range and N_a exceeding 3000 cm^{-3}. The nucleation process driven by afternoon photochemical reactions is the dominant factor controlling the diurnal variation of N_a. From night to early morning, however, nucleation mode particle concentrations are generally below 400 cm^{-3}, which is directly related to the cessation of photochemical reactions and the lack of fresh particle supply during the night (Figure 3a).

Although the diurnal peak of the M_a size distribution occurs synchronously with that of N_a at around 16:00, the contributing particle sizes are clearly different, with the mass mainly coming from accumulation mode particles larger than 100 nm. Freshly formed ultrafine particles in the afternoon can hardly grow to large sizes within a short time. The high M_a values mainly originate from aged, large particles transported upward by the lifting of the boundary layer. Meanwhile, previously

https://doi.org/10.5194/egusphere-2026-5590
Preprint. Discussion started: 10 November 2026
© Author(s) 2026. CC BY 4.0 License.

formed particles develop into accumulation mode particles through hygroscopic growth and coagulation, jointly contributing to the M_a peak within the day (Figure 3b).

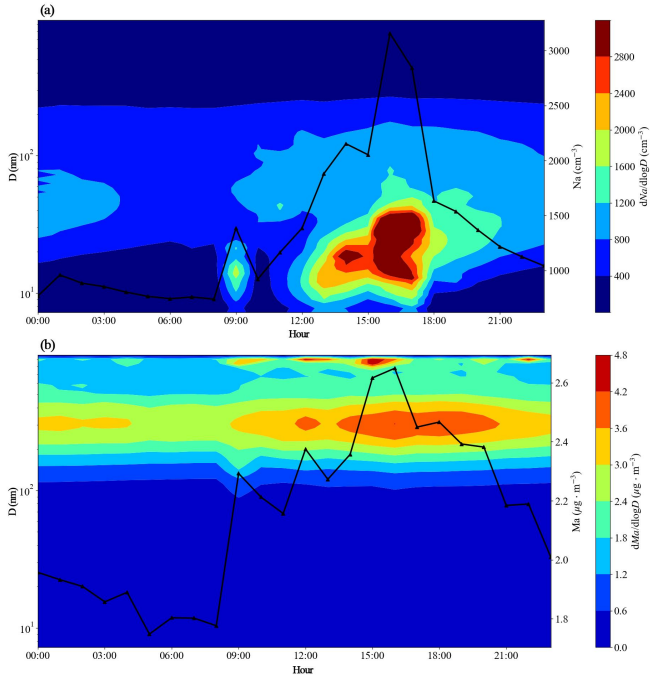


Figure 3: Diurnal variations of (a) N_a and its size distribution, and (b) M_a and its size distribution.

Figure 4 shows the diurnal variation and size distribution characteristics of N_a in different seasons over the LM area. From the diurnal variation (Figure 4a), all four seasons exhibit a unimodal diurnal cycle with an afternoon peak, but with pronounced seasonal differences. Autumn has the highest overall N_a level, with the afternoon peak exceeding 5000 cm^{-3} around 16:00 and a rapid increase starting from 8:00, indicating a strong new particle formation event. Spring has the next highest Na, with the afternoon peak remaining between 2000 and 2500 $cm^{-3}$and a relatively gentler diurnal trend. In summer, due to strong wet scavenging, the afternoon peak is suppressed to about 2000 cm^{-3}. Winter has the lowest N_a throughout the year, with the peak reaching only about 1500 cm^{-3} and the weakest diurnal amplitude.

The size distributions and bimodal fitting results show that in spring (Figure 4b), the main peak of the size distribution is located in the nucleation mode at approximately 18 nm, with a weaker secondary peak at about 80 nm. This indicates that spring is dominated by new particle formation, with a small number of grown Aitken mode particles also present. In autumn (Figure 4d), the main peak is located near 25 nm, and the spectral width is distinctly wider than in spring, suggesting that newly formed particles in autumn have a longer residence time in the atmosphere. In summer (Figure 4c), the main peak is still in the Aitken mode at about 50 nm, but the entire size distribution shifts toward larger diameters, reflecting the suppression of new particle formation by strong wet scavenging and the enhancement of hygroscopic growth and secondary

https://doi.org/10.5194/egusphere-2026-5590
Preprint. Discussion started: 10 November 2026
© Author(s) 2026. CC BY 4.0 License.

transformation of existing particles. In winter (Figure 4e), the size distribution shows a clear bimodal structure, with the nucleation mode (about 20 nm) and the Aitken mode (about 100 nm) having comparable peak intensities. The nucleation mode peak is significantly weaker than in the other three seasons, indicating that new particle formation is suppressed by dry and cold air masses in winter, and the aerosol is dominated by aged and grown Aitken mode particles.

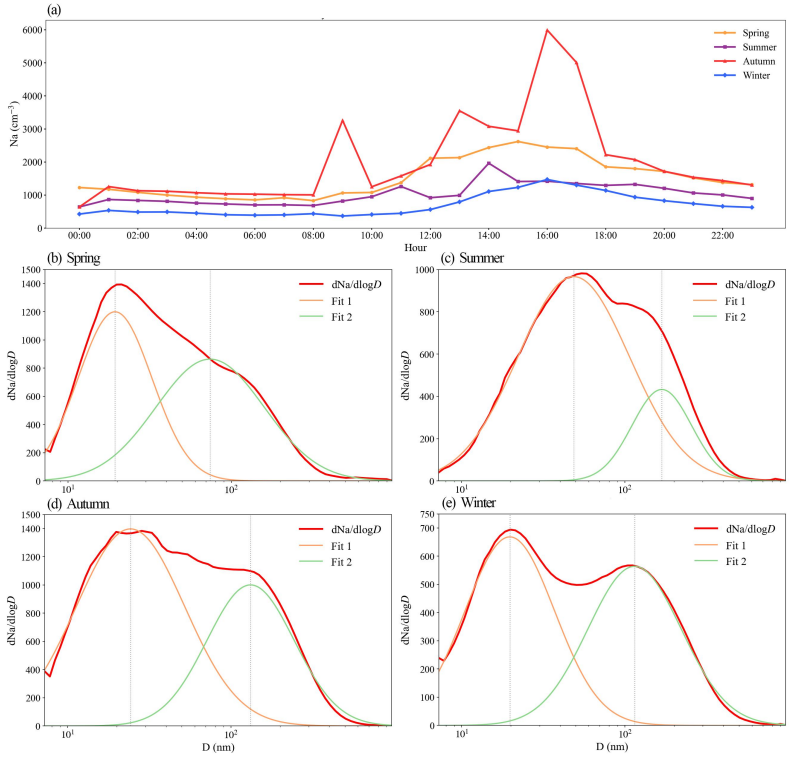


Figure 4: (a) Diurnal variation and (b-e) size distributions of N_a in different seasons.

4 Characteristics of submicron aerosol size distribution under different weather conditions

Based on the seasonal variations of aerosols presented above, it can be seen that atmospheric environmental conditions significantly influence the properties of aerosol particles. To further examine this, we compared the size distribution characteristics of submicron aerosols under different weather conditions.

Figure 5 shows the fractions of different aerosol modes clear days, fog days, and rainy days. On clear days, driven by strong solar radiation and photochemical reactions, new particle formation is relatively active. The nucleation mode fraction is the highest among the three weather conditions, approaching 20%. The Aitken mode and accumulation mode fractions are 43% and 37%, respectively. Overall, the distribution is dominated by the Aitken mode, followed by the accumulation mode and then the nucleation mode, reflecting that under sunny conditions, new particle formation and subsequent growth proceed simultaneously, with particles gradually transforming from the nucleation mode to the Aitken mode and then to the

https://doi.org/10.5194/egusphere-2026-5590
Preprint. Discussion started: 10 November 2026
© Author(s) 2026. CC BY 4.0 License.

accumulation mode. On fog days, the high humidity environment suppresses new particle formation, and the nucleation mode fraction drops to less than 5%. Water vapor promotes hygroscopic growth and coagulation of particles, causing the accumulation mode fraction to rise to its highest value among the three weather conditions, approximately 46%. Overall, the Aitken and accumulation modes dominate, exhibiting a distinct shift toward larger particle sizes. On rainy days, the wet scavenging process shows a marked size dependent effect on particle removal. The nucleation mode fraction also falls below 5%, while the accumulation mode fraction decreases to about 25%, and the Aitken mode fraction exceeds 70%. This indicates that precipitation removes accumulation mode particles, which are larger in size, more efficiently, making the Aitken mode the absolutely dominant aerosol mode under rainy conditions.

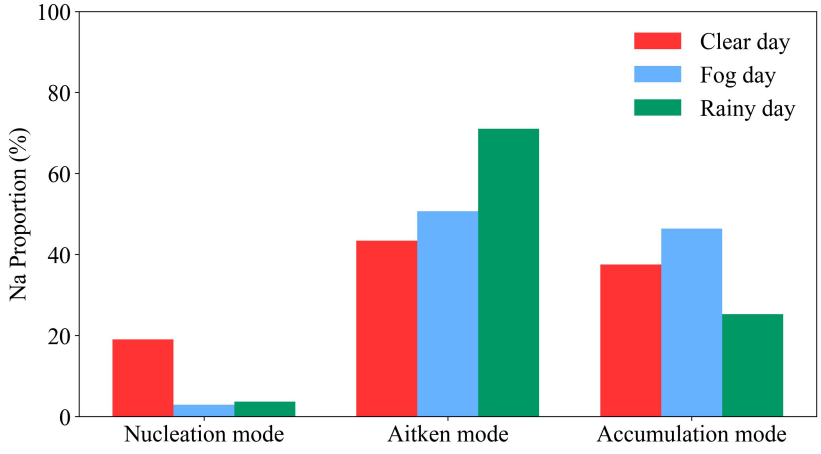


Figure 5: Fractions of different aerosol modes on clear days, fog days, and rainy days.

Figure 6 further presents the size distributions of N_a under different weather conditions. The differences in these distributions correspond closely to the modal fraction characteristics described above. On clear days, the size distribution exhibits a typical bimodal structure, with the highest overall N_a. The two main peaks are located at approximately 45 nm and 620 nm, respectively, reflecting both active new particle formation and initial growth, as well as a notable contribution from background aged particles. On fog days, N_a is significantly lower than on clear days. The size distribution shows a unimodal shape with a broad width, and the peak is located at about 180 nm. The concentration decays much more slowly in the large size range compared to rainy days, reflecting the effects of fog droplets on particle adsorption, enrichment, and growth promotion. On rainy days, N_a is the lowest among the three weather conditions. The size distribution is unimodal, with a peak at about 150 nm and a peak N_a of approximately 650 cm^{-3}, followed by a rapid decrease for particle sizes larger than 150 nm. This feature is directly associated with the scavenging effect of precipitation. On one hand, the inertial impaction of raindrops removes accumulation mode particles more efficiently, leading to a marked reduction in particle concentration in the large size range. On the other hand, new particle formation is suppressed, nucleation mode particles are almost absent,

https://doi.org/10.5194/egusphere-2026-5590
Preprint. Discussion started: 10 November 2026
© Author(s) 2026. CC BY 4.0 License.

and only a portion of nucleation mode particles that have grown hygroscopically into the Aitken mode remain, making the Aitken mode the sole dominant mode in the size distribution.

In summary, the pronounced differences in aerosol size distribution among clear, fog, and rainy days essentially result from the combined effects of particle formation, hygroscopic growth, and size selective wet scavenging under different weather conditions, clearly demonstrating the regulatory influence of local atmospheric environments on aerosol evolution.

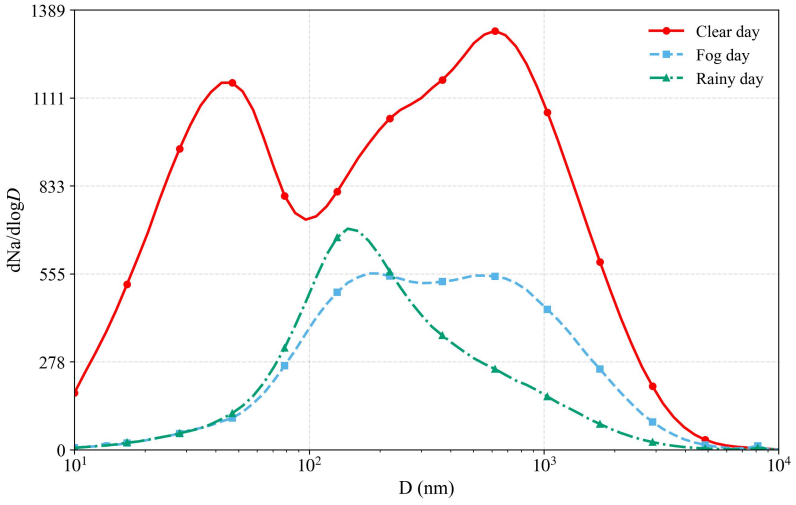


Figure 6: Size distributions of N_a under different weather conditions

5 Impact of submicron aerosols on clouds and fog

In the previous sections, we analyzed the size distribution and evolution characteristics of aerosols under different weather conditions. In fact, aerosols are not merely passively affected by weather processes, they also serve as key drivers of cloud and fog formation. Next, we focus on the regulating role of submicron Na, acting as CCN, on microphysical properties such as fog droplet number concentration (Nf) and droplet diameter.

We conducted synchronous measurements using a CCN counter and a fog droplet spectrometer in the LM area for nearly one month. Figure 7 shows the time series of N_a and N_{CCN} at different supersaturation ratios from September 1 to 21, 2024. As seen in Figure 7a, during the observation period, N_a and M_a exhibit a pronounced synchronous fluctuation pattern overall. High N_a periods (e.g., September 3 and September 15) correspond to peaks in M_a, while on days with low N_a, such as September 5 and September 21, M_a also drops to relatively low levels. The highly consistent trends between the two reflect that during the observation period, the aerosol is dominated by regional background and local emissions, with an intrinsic consistency between N_a and M_a variations.

https://doi.org/10.5194/egusphere-2026-5590
Preprint. Discussion started: 10 November 2026
© Author(s) 2026. CC BY 4.0 License.

From the perspective of the daily variation of N_{CCN} at different supersaturation (SS) levels (Figure 7b), the N_{CCN} shows a highly consistent synchronous fluctuation with Na. This indicates that N_a is the key factor controlling CCN concentration in this region, and its variation directly regulates the total number of particles available for cloud and fog activation. Moreover, comparing different SS levels, N_{CCN} increases as SS rises from 0.2% to 1.0%, and the differences among different SS levels are more pronounced during high N_a periods. This suggests that under conditions of high aerosol concentration, increasing supersaturation can activate more particles with weaker hygroscopicity, thereby amplifying the influence of aerosols on CCN concentration.

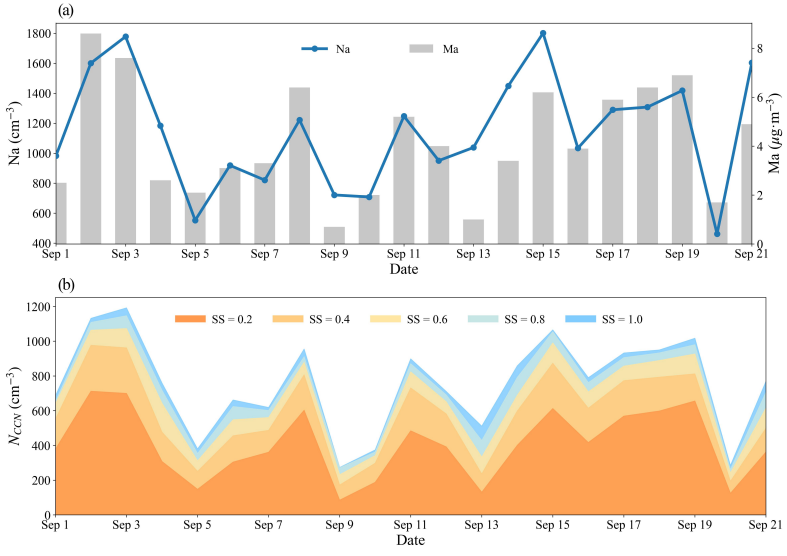


Figure 7: Time series of (a) N_a and (b) CCN number concentrations (N_{CCN}) at different supersaturation ratios from September 1 to 21, 2024

Figure 8 presents the relationships between N_a of different modes and N_{CCN} at different supersaturation ratios. For nucleation mode aerosols, the correlation between nucleation mode particle concentration and N_{CCN} is extremely low at all supersaturation levels (SS from 0.2% to 1.0%), indicating that the contribution of nucleation mode particles to CCN is nearly negligible during the observation period. For Aitken mode particles, the correlation with N_{CCN} improves compared to the nucleation mode, with correlation coefficients r ranging from 0.12 to 0.33, showing a weak positive trend overall. As supersaturation increases, the correlation strengthens slightly, but none reaches a statistically significant level. This suggests that Aitken mode particles have a certain contribution to CCN, but limited by their size and hygroscopicity, they are not the main source of CCN in this region. Distinct from the previous two modes, accumulation mode particles exhibit a strong, significant positive correlation with N_{CCN} at all supersaturation levels, with correlation coefficients r reaching 0.96 to 0.99, all passing significance tests. The fitting slopes also increase with rising supersaturation. These results clearly demonstrate that accumulation mode particles are the absolutely dominant source of CCN in the observed region, and variations in their number concentration directly determine the level of N_{CCN} under different supersaturation conditions.

https://doi.org/10.5194/egusphere-2026-5590
Preprint. Discussion started: 10 November 2026
© Author(s) 2026. CC BY 4.0 License.

Overall, the contributions of the three aerosol modes to CCN are distinctly different. The nucleation mode contributes almost nothing, the Aitken mode contributes weakly, and the accumulation mode is the key factor controlling N_{CCN}. This further explains the highly synchronous variation between N_a and N_{CCN} concentration observed during the measurement period, which is essentially due to the dominant role of accumulation mode particles.

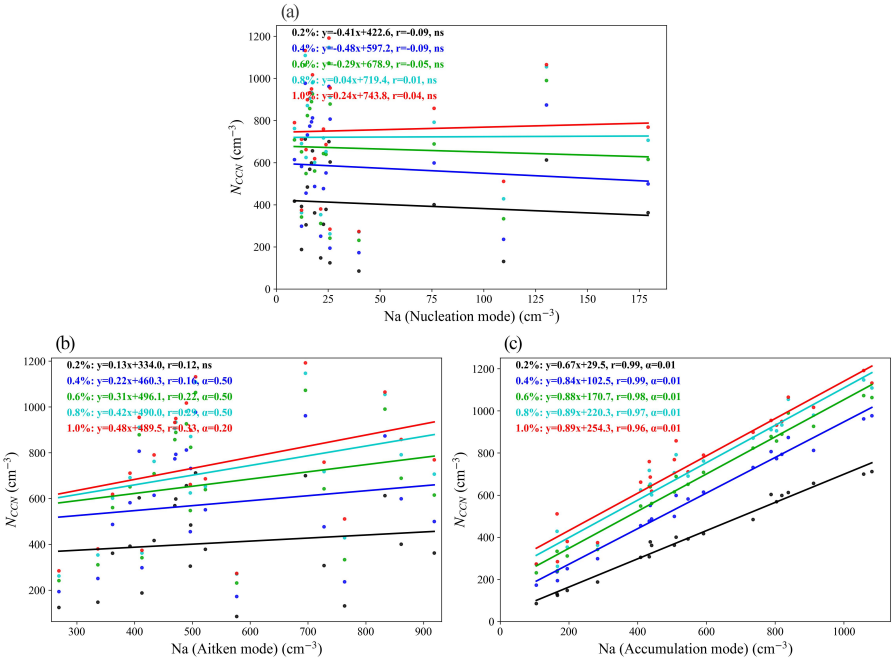


Figure 8: Correlations between N_a of different modes and N_{CCN} at different supersaturation ratios.

Figure 9 shows the variation of aerosol CCN activation efficiency under different supersaturation ratios. The results clearly reflect the significant regulating effect of supersaturation on the particle activation process. As supersaturation increases from 0.2% to 1.0%, the overall activation efficiency of aerosols gradually rises from 35.44% to 65.67%. This indicates that at low supersaturation, only particles with stronger hygroscopicity and larger sizes can be activated, whereas under high supersaturation conditions, some Aitken mode particles can also participate in the activation process.

Overall, the variation of CCN concentration in this region is mainly governed by the concentration level of accumulation mode aerosols. Supersaturation conditions further influence the actual number of cloud condensation nuclei involved in cloud and fog formation by regulating the activation fraction of particles with different sizes and hygroscopicities.

https://doi.org/10.5194/egusphere-2026-5590
Preprint. Discussion started: 10 November 2026
© Author(s) 2026. CC BY 4.0 License.

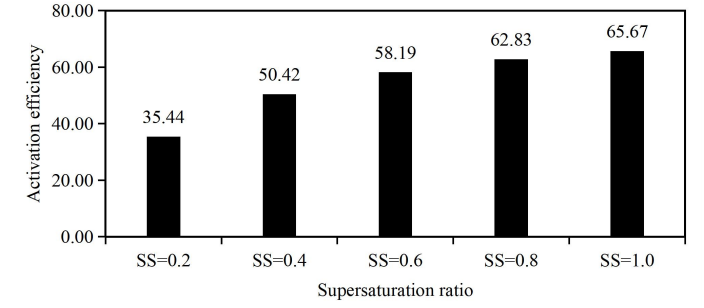


Figure 9: Variation of aerosol CCN activation efficiency under different supersaturation ratios.

Figure 10 presents the relationships between N_a and N_f, liquid water content (LWC), and median volume diameter (MVD). As shown in Figure 10a, N_f exhibits a significant positive correlation with Na, indicating that higher aerosol concentrations provide more CCN that can be activated into fog droplets, directly promoting an increase in Nf. In contrast, LWC shows a significant negative correlation with N_a in Figure 10b, and MVD also decreases notably with increasing N_a in Figure 10c. These results indicate that under high aerosol loading, numerous condensation nuclei compete for limited water vapor, leading to a fog droplet size distribution characterized by many small droplets, thereby reducing individual droplet size and LWC. Conversely, under low aerosol conditions, N_f is low, and water vapor tends to condense onto fewer nuclei, producing fewer but larger droplets with higher LWC. These findings are highly consistent with the CCN activation behavior described above and collectively demonstrate the regulatory effect of aerosols on the microphysical characteristics of clouds and fog.

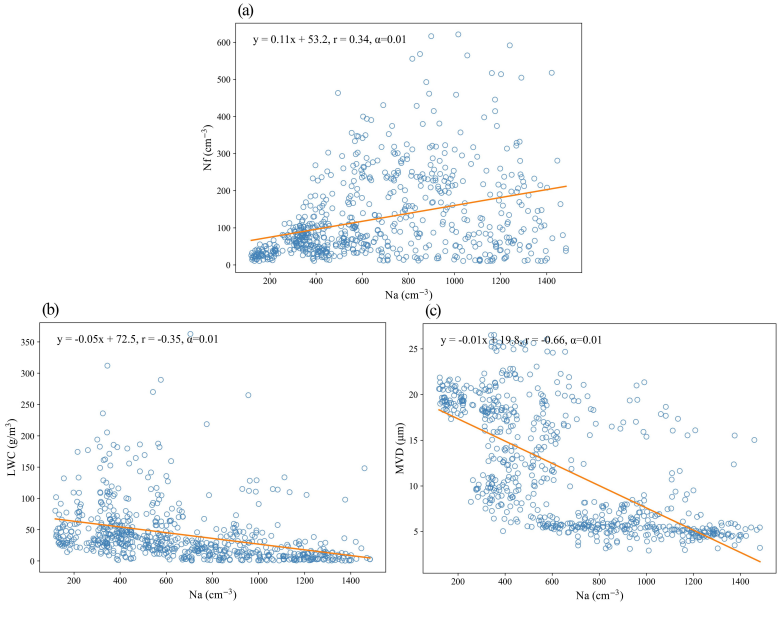


Figure 10: Correlations between N_a and N_f, LWC, and MVD.

https://doi.org/10.5194/egusphere-2026-5590
Preprint. Discussion started: 10 November 2026
© Author(s) 2026. CC BY 4.0 License.

To further analyze the role of aerosols in different stages of a fog event and the effect of fog droplet activation on aerosol concentration, a fog process occurring from September 16 to 17, 2024 was selected for detailed analysis. The time series evolution clearly shows that changes in aerosol and fog microphysical characteristics correspond closely to the fog formation and dissipation stages, with distinctly different particle behavior in each stage.

During the fog formation stage (19:00-23:00 on September 16), nighttime cooling led to a rapid increase in relative humidity, a marked decrease in visibility, and the onset of fog. At this time, N_a remained at a relatively high level with fluctuating behavior, providing an abundant background of condensation nuclei for fog formation (Figure 11a) . Concurrently, N_{CCN} at different supersaturation levels also remained high and increased with rising supersaturation (Figure 11b) , indicating that a large number of hygroscopic particles had the potential for activation. Correspondingly, N_f increased rapidly, and MVD also increased synchronously (Figure 11d) , reflecting the rapid activation of high concentrations of aerosol particles as CCN, which promoted the formation and initial growth of fog droplets.

During the mature stage of the fog (00:00-08:00 on September 17), relative humidity approached saturation, visibility remained low, and the fog process was most intense. At this stage, N_a showed a decreasing trend and remained at a relatively low level, a direct consequence of the activation of a large number of hygroscopic aerosol particles into fog droplets. Correspondingly, N_{CCN} also decreased synchronously with Na, with the decline being particularly pronounced at low supersaturation (SS = 0.2%), indicating that the most readily activated hygroscopic particles had been preferentially consumed. During this stage, N_f first remained at a relatively high level and then decreased significantly, while MVD consistently showed fluctuating high values, indicating that water vapor continued to condense and grow mainly on existing fog droplets, the activation of new particles weakened, and the fog droplet size distribution evolved toward larger diameters.

In the dissipation stage (after 09:00 on September 17), as solar radiation intensified and relative humidity decreased, visibility recovered and fog droplets began to evaporate. In Figure 11a, N_a gradually increased with fog droplet evaporation, and aerosol particles previously embedded in fog droplets were released back into the air, with background concentrations even exceeding those before the fog event. N_{CCN} also recovered synchronously with Na, and the differences in N_{CCN} among different supersaturation levels reappeared, indicating that the hygroscopic characteristics of aerosol particles were restored after fog droplet evaporation. Meanwhile, N_f decreased rapidly, and MVD also decreased correspondingly, as fog droplets evaporated and converted back into aerosol particles. The entire fog process clearly demonstrates the two-way feedback between aerosols and fog. Aerosols trigger fog formation by providing CCN, while the activation, growth, and evaporation of fog droplets in turn modulate the concentration and distribution of aerosols.

https://doi.org/10.5194/egusphere-2026-5590
Preprint. Discussion started: 10 November 2026
© Author(s) 2026. CC BY 4.0 License.

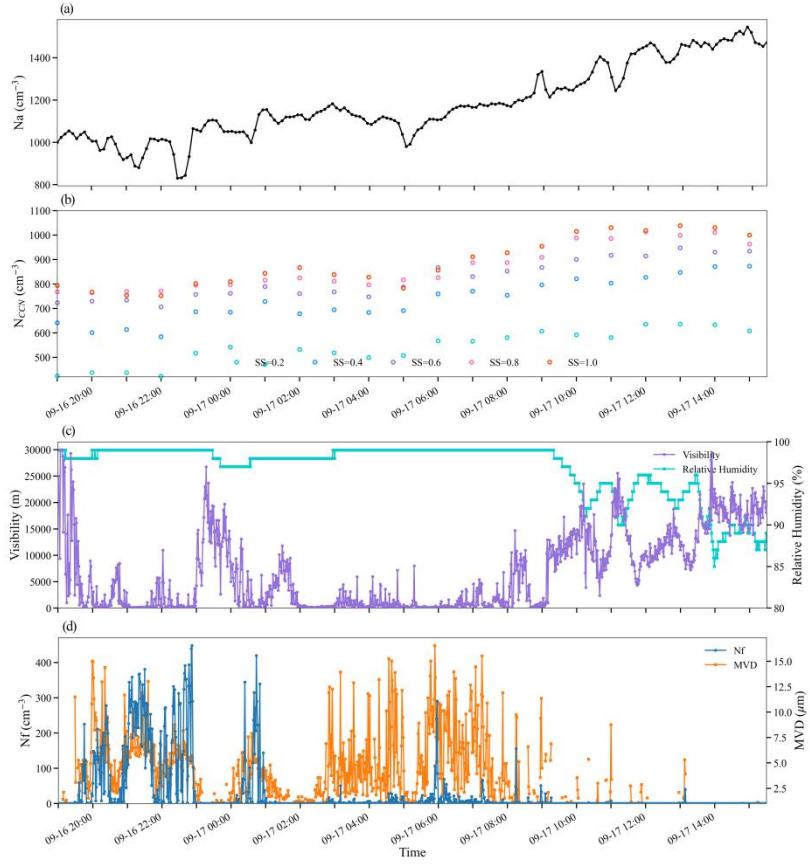


Figure 11: Time series of (a) N_a, (b) N_{CCN} at different supersaturation ratios, (c) visibility and relative humidity, and (d) N_f and MVD from 19:00 on September 16 to 15:00 on September 17, 2024.

6 Conclusions and discussions

In this study, multi-source in situ observations were used to investigate the multi-timescale evolution of submicron aerosols, their size distribution characteristics under different weather conditions, as well as their activation properties and subsequent effects on cloud and fog microphysical processes. N_a and M_a over the LM area exhibit significant seasonal differences. The peak N_a occurs in late autumn and late spring, reaching above 3000 cm^{-3}, mainly contributed by freshly formed particles in the nucleation and Aitken modes. In contrast, the peak M_a is concentrated in late summer, reaching 12.0 $\mu g/m^3$ in early August. This can be attributed to the fact that while strong wet scavenging in summer suppresses new particle formation, the remaining particles undergo hygroscopic growth and secondary transformation, leading to an increased accumulation mode fraction. In winter, dominated by dry and cold air masses with suppressed photochemical reactions, N_a drops to its annual minimum of 688.44 cm^{-3}. On clear days, active new particle formation results in a bimodal size distribution. On fog days, high humidity promotes particle hygroscopic growth, with the accumulation mode fraction reaching approximately 46%. On

https://doi.org/10.5194/egusphere-2026-5590
Preprint. Discussion started: 10 November 2026
© Author(s) 2026. CC BY 4.0 License.

rainy days, wet scavenging removes accumulation mode particles most efficiently, making the Aitken mode the absolute dominant mode with a fraction exceeding 70%.

Further analysis of aerosol regulation on clouds and fog reveals that accumulation mode particles are the dominant source of CCN in the LM area. N_a shows an extremely strong positive correlation with N_{CCN} at different supersaturation levels, with correlation coefficients ranging from 0.96 to 0.99. In contrast, the contributions of nucleation and Aitken mode particles are weak or negligible. As supersaturation increases from 0.2% to 1.0%, the overall aerosol activation efficiency rises from 35.44% to 65.67%. Under high aerosol loading, the competition of numerous CCN for limited water vapor leads to an increase in N_f but significant reductions in MVD and LWC, forming a "many but small" fog droplet size distribution. Analysis of a typical fog event shows that during the initial stage of fog formation, aerosols are activated into fog droplets. During the mature stage, N_a decreases due to activation consumption, and during the dissipation stage, fog droplet evaporation causes N_a to recover.

The above results systematically elucidate the evolution of submicron aerosols and their regulatory mechanisms on cloud and fog microphysics over the LM area, providing key in situ observational evidence for understanding mountain cloud and fog formation and the indirect climatic effects of aerosols. Nevertheless, certain limitations exist in this study. On the one hand, the synchronous observation period of aerosols and cloud/fog is relatively short, which precludes a comprehensive comparison of the seasonal differences in aerosol-cloud-fog feedback mechanisms. Long-term continuous observations across seasons are needed in the future to complete the analysis of aerosol-cloud-fog interactions throughout the year. On the other hand, this study investigates aerosol activation only from the perspective of particle size mode, without concurrent measurements of aerosol chemical composition. Given that chemical components such as sulfates, nitrates, and organic matter are key factors determining particle hygroscopicity and CCN activation efficiency, we cannot further distinguish the synergistic effects of particle size and chemical composition on activation. Future research should integrate multi-platform, long-term observations and numerical modeling to further unravel the complex mechanisms of aerosol-cloud-fog interactions over the LM area.

Data availability

The datasets used in this analysis are available on Zenodo at https://doi.org/10.5281/zenodo.24096408 (Luo et al., 2026).

Author contributions

ZS and YL conceived and designed the study. RL made measurements, analyzed the data, and wrote the original draft. ZC, FL, and LJ conducted the field campaigns. JM and LT directed the manuscript development and editing. ZD and LL provided the fog and CCN data. LX and ZS contributed to the interpretation and manuscript editing and commenting.

https://doi.org/10.5194/egusphere-2026-5590
Preprint. Discussion started: 10 November 2026
© Author(s) 2026. CC BY 4.0 License.

Competing interests

The authors declare that they have no known competing financial interests or personal relationships that could have appeared to influence the work reported in this paper.

Disclaimer

Publisher's note: Copernicus Publications remainsneutral with regard to jurisdictional claims made in the text, pub-lished maps, institutional affiliations, or any other geographical rep-resentation in this paper. While Copernicus Publications makes every effort to include appropriate place names, the final responsibilitylies with the authors.

Financial support

This research was mainly supported by the Natural Science Foundation of Ningxia (2025AAC030326) and National Natural Science Foundation of China (U22A20577) .

References

Adhikari, P., and Mejia, J.F.: Impact of transported dust aerosols on precipitation over the Nepal Himalayas using convection-permitting WRF-Chem simulation, Atmos. Environ., 15, 100179, https://doi.org/10.1016/j.aeaoa.2022.100179, 2022.

Adhikari, P., and Mejia, J.F.: Aerosol-precipitation elevation dependence over the central Himalayas using cloud-resolving WRF-Chem numerical modeling, Atmos. Chem. Phys., 23, 1019–1042, https://doi.org/10.5194/acp-23-1019-2023, 2023.

Albrecht, B.A.: Aerosols, cloud microphysics, and fractional cloudiness, Science, 245, 1227 – 1230, https://doi.org/10.1126/science.245.4923.1227, 1989.

Barahona, D., Sotiropoulou, R., and Nenes, A.: Global distribution of cloud droplet number concentration, autoconversion rate, and aerosol indirect effect under diabatic droplet activation, J. Geophys. Res., 116, D09203, https://doi.org/10.1029/2010JD015274, 2011.

Barman, N., and Gokhale, S.: Aerosol influence on the pre-monsoon rainfall mechanisms over North-East India: A WRF-Chem study, Atmos. Res., 268, 106002, https://doi.org/10.1016/j.atmosres.2021.106002, 2022.

Bellouin, N., Quaas, J., Gryspeerdt, E., Kinne, S., Stier, P., Watson-Parris, D., Boucher, O., Carslaw, K.S., Christensen, M., Daniau, A.-L., Dufresne, J.-L., Feingold, G., Fiedler, S., Forster, P., Gettelman, A., Haywood, J.M., Lohmann, U., Malavelle, F., Mauritsen, T., McCoy, D.T., Myhre, G., Mülmenstädt, J., Neubauer, D., Possner, A., Rugenstein, M., Sato, Y., Schulz, M., Schwartz, S.E., Sourdeval, O., Storelvmo, T., Toll, V., Winker, D., and Stevens, B.: Bounding global aerosol radiative forcing of climate change, Rev. Geophys., 58, e2019RG000660, https://doi.org/10.1029/2019RG000660, 2020.

https://doi.org/10.5194/egusphere-2026-5590
Preprint. Discussion started: 10 November 2026
© Author(s) 2026. CC BY 4.0 License.

Cao, N., Yao, Z., Shu, Z., Chang, Z., Mu, J., Zhu, H., and Lin, T.: Topographic effects on stratiform precipitation observed by vertically pointing micro rain radars at ridge and valley sites in the Liupan Mountains area, northwest China, Water, 15, 134, https://doi.org/10.3390/w15010134, 2023.

Chang, Z., Cui, Y., Tian, L., Dai, Y., Jia, L., Li, L., Zhou, N., and Ma, S.: Observing cloud base height variations in the complex orographic transition zone between the Loess Plateau and the Inner Mongolia Plateau using a ceilometer, SOLA, 22, 22, https://doi.org/10.1007/s44393-026-00022-2, 2026.

Dagan, G., Yeheskel, N., and Williams, A.I.L.: Radiative forcing from aerosol-cloud interactions enhanced by large-scale circulation adjustments, Nat. Geosci., 16, 1092–1098, https://doi.org/10.1038/s41561-023-01319-8, 2023.

Duan, J., Chen, Y., Zhang, X., Wang, W., Zhong, S., Li, J., Lu, G., Fang, C., Guo, L., and Fu, P.: Influence of aerosol physicochemical properties on CCN activation during the Asian winter monsoon at the summit of Mt. Lu, China, Atmos. Environ., 296, 119592, https://doi.org/10.1016/j.atmosenv.2023.119592, 2023.

Fan, J., Rosenfeld, D., Zhang, Y., Giangrande, S. E., Li, Z., Machado, L. A. T., Martin, S. T., Yang, Y., Wang, J., Artaxo, P., Barbosa, H. M. J., Braga, R. C., Comstock, J. M., Feng, Z., Gao, W., Gomes, H. B., Mei, F., Pohler, C., Pohler, M. L., and de Souza, R. A. F.: Substantial convection and precipitation enhancements by ultrafine aerosol particles, Science, 359, 411-418, https://doi.org/10.1126/science.aan8461, 2018.

Fast, J.D., Varble, A.C., Mei, F., Pekour, M., Tomlinson, J., Zelenyuk, A., Sedlacek III, A.J., Zawadowicz, M., and Emmons, L.: Large spatiotemporal variability in aerosol properties over central Argentina during the CACTI field campaign, Atmos. Chem. Phys., 24, 13477–13502, https://doi.org/10.5194/acp-24-13477-2024, 2024.

Feldman, D.R., Aiken, A.C., Boos, W.R., Carroll, R.W.H., Chandrasekar, V., Collis, S., Creamean, J.M., de Boer, G., Deems, J., DeMott, P.J., Fan, J., Flores, A.N., Gochis, D., Grover, M., Hill, T.C.J., Hodshire, A., Hulm, E., Hume, C.C., Jackson, R., Junyent, F., Kennedy, A., Kumjian, M., Levin, E.J.T., Lundquist, J.D., O'Brien, J., Raleigh, M.S., Reithel, J., Rhoades, A., Rittger, K., Rudisill, W., Sherman, Z., Siirila-Woodburn, E., Skiles, S.M., Smith, J.N., Sullivan, R.C., Theisen, A., Tuftedal, M., Varble, A.C., Wiedlea, A., Wielandt, S., Williams, K., and Xu, Z.: The Surface-Atmosphere Integrated Field Laboratory (SAIL) campaign, Bull. Am. Meteorol. Soc., 104, E2192 – E2222, https://doi.org/10.1175/BAMS-D-22-0049.1, 2023.

Gao, M., Zhou, S., Li, W., Li, F., Teng, X., Li, Y., He, Y., Hang, J., and Wang, X.: Formation and evolution of secondary aerosols at a mountain site in southeastern China: Impacts of dust transport and cloud processes, J. Geophys. Res. Atmos., 130, e2025JD044568, https://doi.org/10.1029/2025JD044568, 2025.

Georgakaki, P., Bougiatioti, A., Wieder, J., Mignani, C., Ramelli, F., Kanji, Z.A., Henneberger, J., Hervo, M., Berne, A., Lohmann, U., and Nenes, A.: On the drivers of droplet variability in alpine mixed-phase clouds, Atmos. Chem. Phys., 21, 10993–11012, https://doi.org/10.5194/acp-21-10993-2021, 2021.

Gibson, L.D., Levin, E.J.T., Emerson, E., Good, N., Hodshire, A., McMeeking, G., Patterson, K., Rainwater, B., Ramin, T., and Swanson, B.: Measurement report: An investigation of the spatiotemporal variability in aerosols in the mountainous

https://doi.org/10.5194/egusphere-2026-5590
Preprint. Discussion started: 10 November 2026
© Author(s) 2026. CC BY 4.0 License.

terrain of the upper Colorado River basin using SAIL-Net, Atmos. Chem. Phys., 25, 2745–2760, https://doi.org/10.5194/acp-25-2745-2025, 2025.

He, Y., Shu, Z.L., Zheng, J.F., Jia, X.C., Qiu, Y.J., Deng, P.Y., Yan, X., Lin, T., Dang, Z.L., and Lu, C.S.: A comparative study on the vertical structures and microphysical properties of a mixed precipitation process over different topographic positions of the Liupan Mountains in northwest China, Atmosphere, 14, 44, https://doi.org/10.3390/atmos14010044, 2023.

Henao, J.J., Mejia, J.F., and McDonough, F.: Impacts of anthropogenic aerosols on orographic precipitation in Arizona, Urban Climate, 49, 101561, https://doi.org/10.1016/j.uclim.2023.101561, 2023.

Hua, S., Liu, Y., Luo, R., Shao, T., and Zhu, Q.: Inconsistent aerosol indirect effects on water clouds and ice clouds over the Tibetan Plateau, Int. J. Climatol., 40, 3832–3848, https://doi.org/10.1002/joc.6430, 2020.

Huang, J., Li, Y., Fu, C., Chen, F., Fu, Q., Dai, A., Shinoda, M., Ma, Z., Guo, W., Li, Z., Zhang, L., Liu, Y., Yu, H., He, Y., Xie, Y., Guan, X., Ji, M., Lin, L., Wang, S., Yan, H., and Wang, G.: Dryland climate change: recent progress and challenges, Rev. Geophys., 55, 719–778, https://doi.org/10.1002/2016RG000550, 2017.

IPCC: Climate Change 2021: The Physical Science Basis. Contribution of Working Group I to the Sixth Assessment Report of the Intergovernmental Panel on Climate Change, Cambridge University Press, Cambridge, https://www.ipcc.ch/report/ar6/wg1/, 2021.

Ji, Z., Wang, Y., Li, J., Zhang, P., Fang, F., Xu, Q., Lv, R., Shi, J., and Huang, J.: In situ observations reveal that the South Asian summer monsoon weakens aerosol cloud activation over the southern Tibetan Plateau, Geophys. Res. Lett., 52, e2025GL118406, https://doi.org/10.1029/2025GL118406, 2025.

Jung, W., Sung, H.M., Lee, D.I., Cha, J.W., Chang, K., and Lee, C.: Investigating statistical characteristics of aerosol–cloud interactions over East Asia retrieved from MODIS satellite data, J. Environ. Sci. Int., 29, 1065 – 1078, https://doi.org/10.5322/JESI.2020.29.11.1065, 2020.

Li, J., Carlson, B.E., Yung, Y.L., Lv, D., Hansen, J., Penner, J.E., Liao, H., Ramaswamy, V., Kahn, R.A., Zhang, P., Dubovik, O., Ding, A., Lacis, A., Zhang, L., and Dong, Y.: Scattering and absorbing aerosols in the climate system, Nat. Rev. Earth Environ., 3, 363–379, https://doi.org/10.1038/s43017-022-00296-7, 2022.

Li, L., Li, M., Fan, X., Chen, Y., Lin, Z., Hou, A., Zhang, S., Zheng, R., and Chen, J.: Measurement report: The variation properties of aerosol hygroscopic growth related to chemical composition during new particle formation days in a coastal city of Southeast China, Atmos. Chem. Phys., 25, 3669–3685, https://doi.org/10.5194/acp-25-3669-2025, 2025.

Li, T., Yu, Y., Wang, X., Liu, X., Mao, Q., and Yuan, Y.: A review of aerosol−cloud interactions: mechanisms, climate effects, and observation methods, Atmos. Res., 325, 108267, https://doi.org/10.1016/j.atmosres.2025.108267, 2025.

Lin, T., Shu, Z., Wu, H., Tao, T., Cao, N., Zhu, H., Liu, C., Mu, J., and Tian, L.: Variation characteristics and source analysis of cloud condensation nuclei at the ridge of Liupan Mountain located in western China, Atmosphere, 13, 1483, https://doi.org/10.3390/atmos13091483, 2022.

https://doi.org/10.5194/egusphere-2026-5590
Preprint. Discussion started: 10 November 2026
© Author(s) 2026. CC BY 4.0 License.

Lin, T., Shu, Z.L., Deng, P.Y., Tian, L., Sun, Y.Q., Jia, L., Cao, N., and Bai, H.B.: Vertical distribution of different phase particles in summer topographic clouds over Liupan Mountain, Phys. Chem. Earth, 142, 104212, https://doi.org/10.1016/j.pce.2025.104212, 2025.

Liu, Q., Shen, X., Li, L., Sun, J., Liu, Z., Zhu, W., Zhong, J., Zhang, Y., Hu, X., Liu, S., Che, H., and Zhang, X.: Impacts of aerosol chemical composition on cloud condensation nuclei (CCN) activity during wintertime in Beijing, China, Remote Sens., 15, 4119, https://doi.org/10.3390/rs15174119, 2023.

Liu, Y., Shao, T., Hua, S., Zhu, Q., and Luo, R.: Association of anthropogenic aerosols with subtropical drought in East Asia, Int. J. Climatol., 40, 3500–3513, https://doi.org/10.1002/joc.6410, 2020.

Luo, R., Liu, Y., Luo, M., Li, D., Tan, Z., and Shao, T.: Dust effects on mixed-phase clouds and precipitation during a super dust storm over northern China, Atmos. Environ., 313, 120081, https://doi.org/10.1016/j.atmosenv.2023.120081, 2023.

Motos, G., Freitas, G., Georgakaki, P., Wieder, J., Li, G., Aas, W., Lunder, C., Krejci, R., Pasquier, J.T., Henneberger, J., and Nenes, A.: Aerosol and dynamical contributions to cloud droplet formation in Arctic low-level clouds, Atmos. Chem. Phys., 23, 13941–13956, https://doi.org/10.5194/acp-23-13941-2023, 2023.

Quaas, J., Arola, A., Cairns, B., Christensen, M., and Deneke, H.: Constraining the Twomey effect from satellite observations: Issues and perspectives, Atmos. Chem. Phys., 20, 15079–15099, https://doi.org/10.5194/acp-20-15079-2020, 2020.

Rosenfeld, D., Lohmann, U., Raga, G.B., O'Dowd, C.D., Kulmala, M., Fuzzi, S., Reissell, A., and Andreae, M.O.: Flood or drought: How do aerosols affect precipitation?, Science, 321, 1309–1313, https://doi.org/10.1126/science.1160606, 2008.

Singh, P., Sarawade, P., and Adhikary, B.: Vertical distribution of aerosols during deep-convective event in the Himalaya using WRF-Chem model at convection permitting scale, Atmosphere, 12, 1092, https://doi.org/10.3390/atmos12091092, 2021.

Storelvmo, T. and Tan, I.: The Wegener–Bergeron–Findeisen process – Its discovery and vital importance for weather and climate, Meteorol. Z., 24, 455–461, https://doi.org/10.1127/metz/2015/0626, 2015.

Twomey, S.: Pollution and the planetary albedo, Atmos. Environ., 8, 1251 – 1256, https://doi.org/10.1016/0004-6981(74)90004-3, 1974.

Twomey, S.: The influence of pollution on the shortwave albedo of clouds, J. Atmos. Sci., 34, 1149 – 1152, https://doi.org/10.1175/1520-0469(1977)034<1149:TIOPOT>2.0.CO;2, 1977.

Wehbe, Y., Tessendorf, S.A., Weeks, C., Bruintjes, R., Xue, L., Rasmussen, R., Lawson, P., Woods, S., and Temimi, M.: Analysis of aerosol–cloud interactions and their implications for precipitation formation using aircraft observations over the United Arab Emirates, Atmos. Chem. Phys., 21, 12543–12560, https://doi.org/10.5194/acp-21-12543-2021, 2021.

Xu, J.Z., Mei, F., Zhang, X.H., Zhao, W.H., Zhai, L.X., Zhong, M., and Hou, S.G.: Impact of anthropogenic aerosol transport on cloud condensation nuclei activity during summertime in Qilian Mountain, in the northern Tibetan Plateau, J. Geophys. Res. Atmos., 129, e2023JD040519, https://doi.org/10.1029/2023JD040519, 2024.

https://doi.org/10.5194/egusphere-2026-5590
Preprint. Discussion started: 10 November 2026
© Author(s) 2026. CC BY 4.0 License.

Yang, Y., Fan, J., Leung, L.R., Zhao, C., Li, Z., and Rosenfeld, D.: Mechanisms contributing to suppressed precipitation in Mt. Hua of central China. Part I: Mountain valley circulation, J. Atmos. Sci., 73, 1351–1366, https://doi.org/10.1175/JAS-D-15-0233.1, 2016.

Zhang, G., Peng, X., Sun, W., Fu, Y., and Yang, Y.: Fog/cloud processing of atmospheric aerosols from a single particle perspective: A review of field observations, Atmos. Environ., 329, 120536, https://doi.org/10.1016/j.atmosenv.2024.120536, 2024.

Zhang, J., Zhou, X., Goren, T., and Feingold, G.: Albedo susceptibility of northeastern Pacific stratocumulus: the role of covarying meteorological conditions, Atmos. Chem. Phys., 22, 861–880, https://doi.org/10.5194/acp-22-861-2022, 2022.

Zhang, L., Li, J., Jiang, Z., Dong, Y., Ying, T., and Zhang, Z.: Clear-sky direct aerosol radiative forcing uncertainty associated with aerosol optical properties based on CMIP6 models, J. Clim., 35, 3021–3035, https://doi.org/10.1175/JCLI-D-21-0480.1, 2022.

Zhang, Y., Xu, W., Li, Y., Zhang, G., Liu, D., Kuang, Y., Zhang, Y., Zhou, W., Peng, X., Su, B., Huang, W., Zhang, Z., Yang, L., Wu, Y., Li, S., Zhao, S., Liu, L., Pan, X., Wang, Z., Bi, X., Ehn, M., Worsnop, D. R., and Sun, Y.: Seasonal variability and cloud-type effects on secondary organic aerosol formation during cloud events at a mountainous site in southeastern China, Atmos. Chem. Phys., 26, 5617-5634, https://doi.org/10.5194/acp-26-5617-2026, 2026.